Composition dependence of the structure and the electronic states of liquid K-Pb alloys: ab initio molecular-dynamics simulations

1999 J. Phys.: Condens. Matter 11 5387

(http://iopscience.iop.org/0953-8984/11/28/301)

J. Phys.: Condens. Matter **11** (1999) 5387–5398. Printed in the UK PII: S0953-8984(99)02432-7

Composition dependence of the structure and the electronic states of liquid K–Pb alloys: *ab initio* molecular-dynamics simulations

Y Senda, F Shimojo and K Hoshino

Faculty of Integrated Arts and Sciences, Hiroshima University, Higashi-Hiroshima 739-8521, Japan

Received 5 March 1999

Abstract. We have carried out *ab initio* molecular-dynamics simulations for the compound-forming liquid K–Pb alloys to investigate the composition dependence of their ionic structure and electronic states. It is shown that the tetrahedral Pb_4^{4-} clusters, which are the so-called 'Zintl ions' seen in the crystalline compound KPb, appear for the liquid K-rich alloy, while the Zintl ions are connected to each other and a complex structure is formed for the liquid equiatomic alloy. The observed structure factor characterized by the first sharp diffraction peak can be reproduced and it is found that the prepeak arises from the intermediate-range ordering of the Zintl ions. The composition dependence of the resistivity is well reproduced by means of the Kubo–Greenwood formula and its characteristic features are understood on the basis of the calculated electronic states and the ionic structure obtained.

1. Introduction

Among the liquid alkali–group-14 alloys, which are well known as compound-forming liquid alloys [1–3], the liquid K–Pb alloys have been studied most extensively. The equiatomic crystalline compounds APb (A = Na, K, Rb, Cs) have a structure which includes tetrahedral Pb_4^{4-} clusters, so-called 'Zintl ions', and they are present with high stability, i.e. with a high melting point, as is apparent from their phase diagrams. The formation of the Zintl ion is closely related to the electronic charge transfer from the A atom to the Pb atom, which occurs as a result of the large difference in electronegativity between the two species.

The Zintl ion has been expected to persist even in the liquid alloy, on the basis of the experimental results for the composition dependence of the electrical resistivity, the thermodynamic properties and the structural properties. For the liquid K–Pb alloy, the maximum of the resistivity as a function of the composition appears at $K_{0.5}Pb_{0.5}$ [4], where the so-called first sharp diffraction peak (FSDP) is most pronounced [2]. For the alkali-rich composition, a tendency towards phase separation was found. In addition to this experimental evidence, the FSDP was also observed under extreme thermodynamic conditions [3]. These experimental results have been explained on the basis of the existence of Zintl ions in liquid K–Pb alloys.

A stability rule for the Zintl ion, proposed by Geertsma and van der Lugt [5], states that liquid alkali–Pb alloys with larger alkali atoms contain Zintl ions that are more stable. This rule could explain the observed facts that, on going from K–Pb to Cs–Pb alloy, the maximum of the resistivity at 50% Pb increases rapidly and the height of the FSDP increases. According

0953-8984/99/285387+12$30.00

to this rule, liquid $Cs_{0.5}Pb_{0.5}$ alloy, which contains the largest alkali atom, can be considered to have the most stable Zintl ion among the liquid alkali–Pb alloys.

Recently, an *ab initio* molecular-dynamics (MD) simulation of the liquid $Cs_{0.5}Pb_{0.5}$ alloy was carried out [6] and, contrary to expectation, a more complex structure than that expected in the perfect-Zintl-ion picture was obtained; the configuration of the Pb atoms was described as a disordered network, though it still has many features in common with the Zintl-ion model. We have already applied *ab initio* MD simulation to the liquid Na–Pb alloys to investigate the microscopic structure and electronic states [7]. It was shown by our study that the intermediate-range ordering of Pb ions is the origin of the observed FSDP for the liquid $Na_{0.8}Pb_{0.2}$ alloy and that no Zintl ion was seen as a stable isolated cluster in a network of Pb ions for the liquid $Na_{0.5}Pb_{0.5}$ alloy.

It is of interest to apply *ab initio* MD simulation to the liquid K–Pb alloy, since the alkali K atom is smaller than the Cs atom and larger than the Na atom.

Recently, *ab initio* MD simulation has been applied to a variety of liquid alloys [8–13]; the findings show that this theoretical method is a very effective and successful tool for describing liquid alloys in which the correlation between the ionic configuration and the electronic states plays an important role [14, 15]. A classical MD simulation for the liquid K–Pb alloy has already been carried out [16] and the calculated structure factors appeared to agree fairly well with the observed ones, though a simple ionic–molecular model was used in the calculation. An *ab initio* calculation for an isolated K–Pb cluster [17] indicated a high stability of the Zintl cluster, on the basis of which persistence of the Zintl cluster in the melts was suggested.

In this paper we apply *ab initio* MD simulation to the liquid $K_{0.8}Pb_{0.2}$, $K_{0.5}Pb_{0.5}$ and $K_{0.2}Pb_{0.8}$ alloys. The purposes of this paper are (i) to investigate the composition dependence of the ionic structures and the electronic states, (ii) to investigate the composition dependence of the electrical conductivity by means of the Kubo–Greenwood formula and (iii) to provide a microscopic interpretation for the observed characteristic features.

In section 2 we briefly summarize the method of our *ab initio* MD simulation. In section 3, the results of our calculation are given and discussed in comparison with the experimental results. Finally, our conclusions are given in section 4.

2. Method

To study the structure and the electronic states of liquid K–Pb alloys, we carry out an *ab initio* MD simulation, which is based on the density functional theory in the local-density approximation, the pseudopotential theory and the adiabatic approximation. We minimize the Kohn–Sham energy functional for a given ionic configuration by the conjugate-gradient method [18, 19] and calculate the electron density and the forces acting on ions on the basis of the Hellmann–Feynman theorem.

We use the norm-conserving pseudopotential proposed by Troullier and Martins [20] for both K and Pb atoms. The Pb pseudopotential is generated from the scalar-relativistic atomic calculation [21]. The non-local part is calculated using the Kleinman–Bylander separable form [22]. The exchange–correlation energy is calculated in the local-density approximation [23, 24]. The partial-core correction [25] is taken into account in order to guarantee the transferability of the pseudopotentials employed. The fractional occupancies of the energy levels are introduced in order to ensure the convergence of the electronic states of the metals. The wavefunction, sampled only at the Γ point of the Brillouin zone, is expanded in plane waves and their cut-off energy is 10 Ryd, which is determined so as to converge the total energy to within 1 mRyd/electron.

In our calculations, a cubic supercell is used and the periodic boundary condition is

imposed. The total number of atoms in the supercell is taken to be one hundred. The side of the cubic cell is about 16–18 Å. As an initial configuration, K and Pb atoms are randomly arranged on the simple-cubic lattice.

A constant-temperature MD simulation is carried out using the Nosé–Hoover thermostat technique [26, 27]. The classical equations of motion are solved using the velocity Verlet algorithm. Our simulation is carried out for 14.4 ps with the time step of 3.6 fs after the thermal equilibrium state is achieved. The temperatures are 700 K, 870 K and 700 K for the liquid $K_{0.8}Pb_{0.2}$, $K_{0.5}Pb_{0.5}$ and $K_{0.2}Pb_{0.8}$ alloys, respectively. The observed densities are used in our calculation.

3. Results and discussion

3.1. Structural properties

3.1.1. The ionic configuration. We show in figure 1 snapshots of the ionic configurations for the liquid (a) $K_{0.8}Pb_{0.2}$, (b) $K_{0.5}Pb_{0.5}$ and (c) $K_{0.2}Pb_{0.8}$ alloys obtained by our *ab initio* MD simulations. The bonds between Pb ions are drawn for Pb-ion pairs with separations less than 4 Å, which is the radius of the first coordination shell of $g_{\mathrm{PbPb}}(r)$ as will be shown in figure 2. It is seen for the liquid $K_{0.8}Pb_{0.2}$ alloy that there exist two isolated tetrahedral Pb_4 clusters, which we call Zintl ions below, and that the cluster consisted of more than four Pb ions. We found that these chemical units exist as isolated clusters with high stability and that they do not break within our simulation time. For the liquid $K_{0.5}Pb_{0.5}$ alloy, on the other hand, the isolated Zintl ion is not clearly seen, since the Zintl ions are connected to the adjacent Zintl ions in the Pb network-like structure. The Pb–Pb bonds within the Zintl ion sometimes break and rearrange to form bonds with other Pb ions. For the higher Pb concentration, the liquid $K_{0.2}Pb_{0.8}$ alloy has the dense Pb-ion network structure, as is seen in figure 1(c).

The existence of the chemical bond in the Zintl ion is evident from the partial radial distribution functions $g_{\mathrm{KK}}(r)$ and $g_{\mathrm{PbPb}}(r)$ shown in figure 2. It is seen that the first peak of $g_{\mathrm{PbPb}}(r)$ is highest for the liquid $K_{0.8}Pb_{0.2}$ alloy and that the distributions of Pb ions become broader as the Pb concentration increases. The high first peak of $g_{\mathrm{PbPb}}(r)$ for the liquid $K_{0.8}Pb_{0.2}$ alloy comes from the strong chemical bonds within a stable Zintl ion. The position of the first peak corresponds to the length of the Pb–Pb bonds within the Zintl ion. This first peak becomes lower and broader for the liquid $K_{0.5}Pb_{0.5}$ alloy, which is due to the network-like structure of the Pb ions and the rearrangements of the Pb–Pb bond.

When the Pb concentration increases further, for the liquid $K_{0.2}Pb_{0.8}$ alloy, the partial structure of the Pb ions has features in common with that of pure liquid Pb, as is evident from the fact that the distribution of the Pb ions is similar to that of the pure liquid Pb. The position of the first peak of $g_{\mathrm{PbPb}}(r)$ ($r = 3.1$ Å) slightly shifts to a larger r ($r = 3.2$ Å) and is consistent with that of the pure liquid Pb ($r = 3.25$ Å).

3.1.2. The correlation between the Zintl ions. The distribution functions $P(n)$ for the coordination numbers of Pb atoms around a Pb atom are shown in figure 3, where $P(n)$ is defined as the probability that a Pb ion has n neighbouring Pb ions within the first coordination shell of radius 4 Å. The coordination number is three for the perfect Zintl ion. It is seen from figure 3 that the maximum of $P(n)$ is at threefold coordination for the liquid $K_{0.8}Pb_{0.2}$ alloy, while more Pb atoms accumulate around a Pb atom as the Pb concentration increases. The sharp maximum at threefold coordination for the liquid $K_{0.8}Pb_{0.2}$ alloy results from the existence of isolated Zintl ions as is seen in figure 1(a). For the liquid $K_{0.5}Pb_{0.5}$ alloy, since the Zintl ions are connected to each other in the Pb network-like structure, the distribution of the

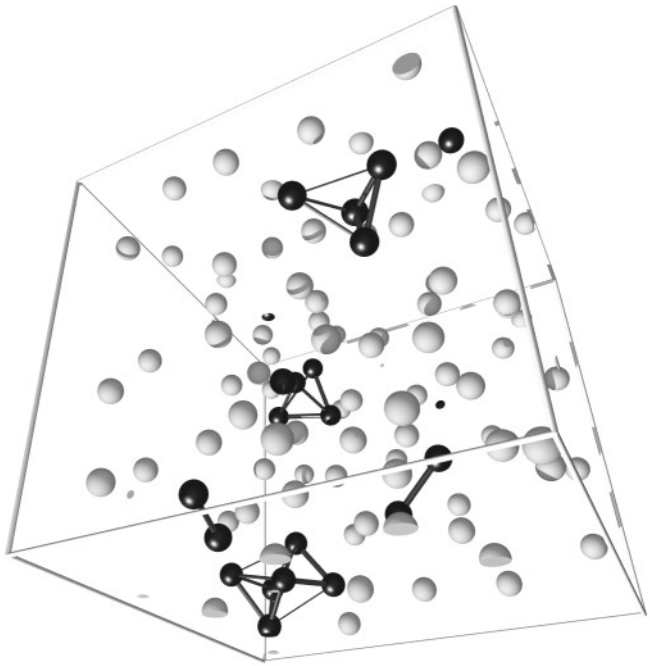

(a)

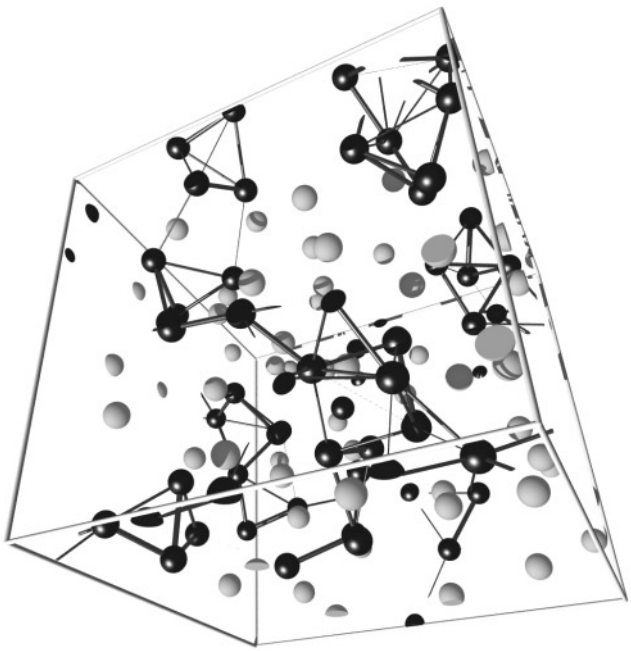

(b)

Figure 1. Snapshots of the ionic configurations for the liquid (a) $K_{0.8}Pb_{0.2}$, (b) $K_{0.5}Pb_{0.5}$ and (c) $K_{0.2}Pb_{0.8}$ alloys. Pb and K ions are shown as black and white balls, respectively. The Pb–Pb bonds are drawn for Pb-ion pairs within the cut-off distance of 4.0 Å.

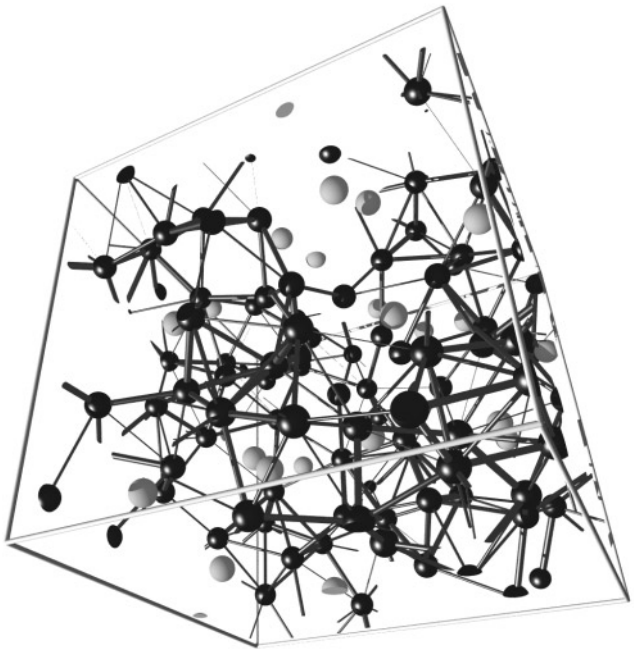

(c)

Figure 1. (Continued)

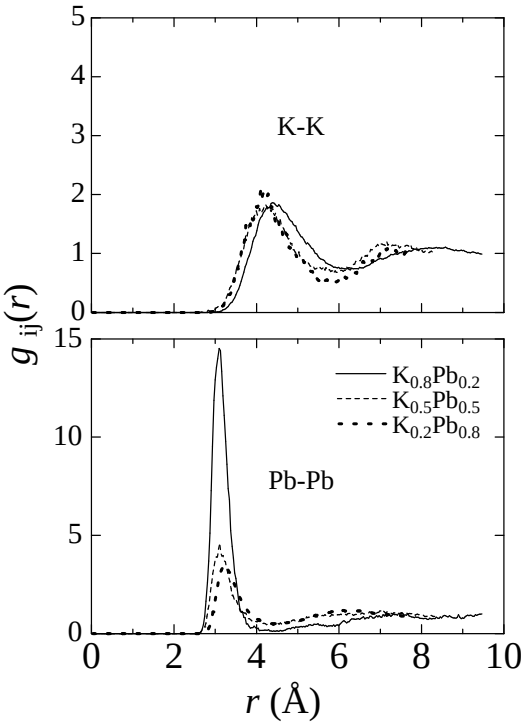

Figure 2. The partial radial distribution functions $g_{KK}(r)$ and $g_{PbPb}(r)$ for the liquid $K_{0.8}Pb_{0.2}$ (solid curves), $K_{0.5}Pb_{0.5}$ (broken curves) and $K_{0.2}Pb_{0.8}$ (dotted curves) alloys.

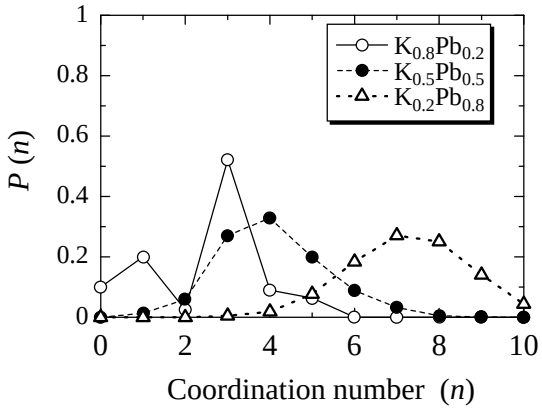

Figure 3. The distribution functions $P(n)$ for the coordination numbers of Pb atoms around a Pb atom for the liquid $K_{0.8}Pb_{0.2}$ (open circles), $K_{0.5}Pb_{0.5}$ (solid circles) and $K_{0.2}Pb_{0.8}$ (open triangles) alloys.

coordination number shifts slightly to larger numbers. When the Pb concentration increases further, the Pb coordination number increases towards that of pure liquid Pb, for which there is no Pb atom which has only three neighbouring Pb atoms.

We find an ordering of the Zintl ions even in the Pb network-like structure which is seen for the liquid $K_{0.5}Pb_{0.5}$ alloy. Here the Zintl ion is defined as the unit of the Pb ions which have three Pb ions within a sphere of radius 4 Å. The radial distribution functions for the centre of mass of the Zintl ion thus defined are shown in figure 4. The short-range correlation within $r = 3$ Å corresponds to that of the adjacent Zintl ion. The intermediate-range ordering of the Zintl ion for the liquid $K_{0.8}Pb_{0.2}$ alloy appears clearly as the peak at around $r \simeq 9$ Å. The corresponding peak appears also for the liquid $K_{0.5}Pb_{0.5}$ alloy, though the distribution is rather broad, which is due to the network-like structure of the Pb ions for this liquid alloy.

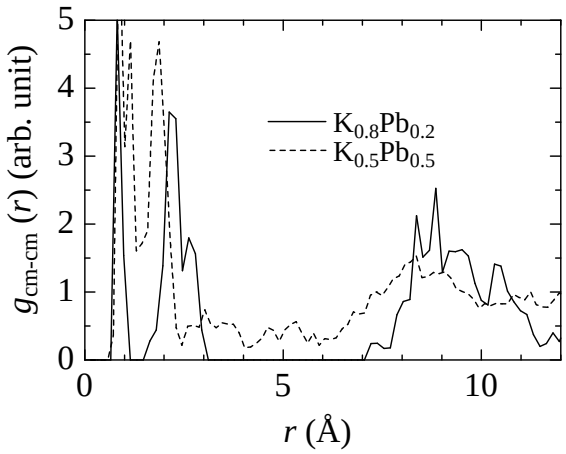

Figure 4. The radial distribution functions of the centre of mass (cm) of the Zintl ion defined for the liquid $K_{0.8}Pb_{0.2}$ (solid curve) and $K_{0.5}Pb_{0.5}$ (broken curve) alloys.

3.1.3. The structure factors. We calculate the total structure factors $S(k)$ in order to compare them with the experimental results obtained by means of neutron diffraction. $S(k)$ is defined by

$$S(k) = \sum_{i,j} (c_i c_j)^{1/2} b_i b_j S_{ij}(k) \Big/ \sum_i c_i b_i^2 \qquad (1)$$

where the c_i and the b_i are, respectively, the concentration and the neutron scattering length of the ith species ($b_K = 0.367 \times 10^{-12}$ cm, $b_{Pb} = 0.940 \times 10^{-12}$ cm) and the $S_{ij}(k)$ are the Ashcroft–Langreth (AL) partial structure factors defined by

$$S_{ij}(k) = \frac{1}{(N_i N_j)^{1/2}} \left\langle \sum_{\mu=1}^{N_i} \sum_{\nu=1}^{N_j} e^{i\boldsymbol{k}\cdot(\boldsymbol{r}_\mu - \boldsymbol{r}_\nu)} \right\rangle \tag{2}$$

using the positions of the ions $\{\boldsymbol{r}_\mu\}$ obtained by our *ab initio* MD simulation. Here N_i is the number of ions of the ith species and the brackets $\langle \cdots \rangle$ mean the time average. Figures 5 and 6 show the calculated total structure factors and the AL partial structure factors, respectively.

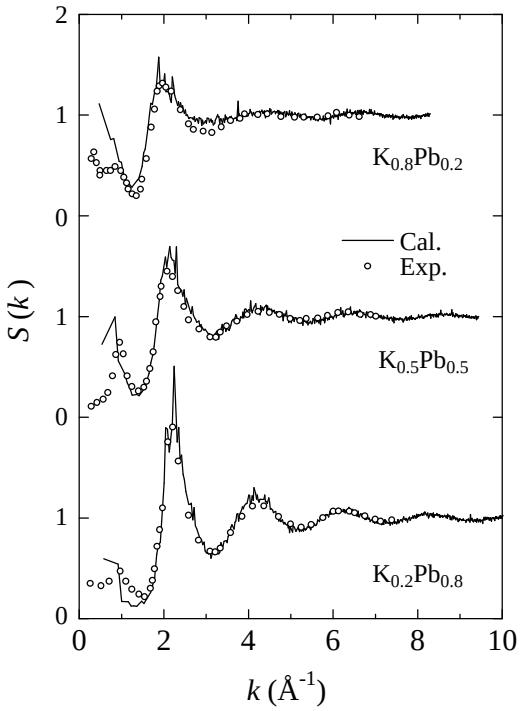

Figure 5. The total structure factors for the liquid $K_{0.8}Pb_{0.2}$, $K_{0.5}Pb_{0.5}$ and $K_{0.2}Pb_{0.8}$ alloys (solid curves). The calculated curves are compared with the results from the neutron scattering experiment (open circles) [2]. The structure factor for the liquid $K_{0.2}Pb_{0.8}$ alloy is compared with that for the composition $K_{0.25}Pb_{0.75}$ from reference [2].

Our calculated total structure factors are in good agreement with the experimental results [2]. In the region where k is lower than $\simeq$1.0 Å^{-1}, there are small differences between the calculated and experimental values, which arise from the limited size of the system used in our calculation, though this quantitative difference may not influence the following discussion.

It is seen from the $S(k)$ that the prepeaks, the so-called FSDP, appear at $k \simeq 0.9$ Å^{-1}; their heights are highest for the liquid $K_{0.5}Pb_{0.5}$ alloy. A shoulder appears at around $k \simeq 2.3$ Å^{-1} for the liquid $K_{0.8}Pb_{0.2}$ alloy. In addition, a tendency towards a large small-angle scattering is apparent for the liquid $K_{0.8}Pb_{0.2}$ alloy and the same effect, though weaker, is also seen for liquid $K_{0.2}Pb_{0.8}$ alloy.

3.1.4. The origin of the FSDP. It is clear that the main contribution to the FSDP of $S(k)$ comes from the prepeak of $S_{PbPb}(k)$. As is seen in equation (1), $S(k)$ can be expressed as a

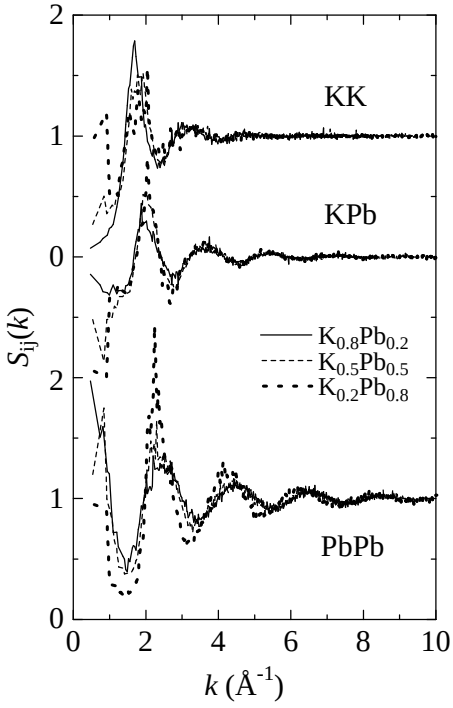

Figure 6. The Ashcroft–Langreth partial structure factors for the liquid $K_{0.8}Pb_{0.2}$ (solid curves), $K_{0.5}Pb_{0.5}$ (broken curves) and $K_{0.2}Pb_{0.8}$ (dotted curves) alloys.

linear combination of the AL partial structure factors. Though there is a prepeak of $S_{KK}(k)$ for the liquid $K_{0.2}Pb_{0.8}$ alloy, it contributes little to the FSDP of $S(k)$, since the ratio of the coefficients for $S_{KK}(k)$ and $S_{PbPb}(k)$ in equation (1) is $c_K b_K^2/c_{Pb} b_{Pb}^2 = 0.15$ for $K_{0.2}Pb_{0.8}$ alloy. Since the value of k at the position of the main peak of $S_{PbPb}(k)$, 2.3 Å^{-1}, is larger than that for $S_{KK}(k)$, 1.9 Å^{-1}, the position of the main peak of $S(k)$ shifts towards that of $S_{PbPb}(k)$ with increasing Pb concentration. For the liquid $K_{0.8}Pb_{0.2}$ alloy, the shoulder of $S(k)$ at around 2.3 Å^{-1} is attributable to the main peak of $S_{PbPb}(k)$, though the contribution to $S(k)$ mainly arises from $S_{KK}(k)$.

The orderings of the Zintl ions in these liquid alloys have significant effects on the structure factors. The prepeaks of $S_{PbPb}(k)$ indicate the occurrence of intermediate-range ordering of Pb ions and the positioning of the prepeaks at $k \simeq 0.9$ Å^{-1} corresponds to the real-space distance $r \simeq 8.5$ Å at which the peak of the radial distribution function for the centre of mass of the Zintl ion (defined in the previous section) was found. The position of the main peaks of $S_{PbPb}(k)$ corresponds to that of the first peak of $g_{PbPb}(r)$ associated with the Pb–Pb bond within the Zintl ion. This is explained if the FSDP at $k \simeq 0.9$ Å^{-1} arises from the intermediate-range correlation between the Zintl ions and the shoulders arise from the Pb–Pb correlation within the Zintl ion.

3.1.5. The concentration fluctuation. The large degree of scattering in the low-k region implies a large concentration fluctuation in the liquid alloy. It is useful to investigate the concentration–concentration structure factor $S_{CC}(k)$, which is defined by

$$S_{CC}(k) = c_K c_{Pb}[c_{Pb} S_{KK}(k) + c_K S_{PbPb}(k) - 2(c_K c_{Pb})^{1/2} S_{KPb}(k)]. \tag{3}$$

The factors $S_{CC}(k)$ for three liquid alloys are shown in figure 7. For the liquid $K_{0.8}Pb_{0.2}$ and $K_{0.2}Pb_{0.8}$ alloys, the large values of $S_{CC}(k)$ in the low-k region indicate a large concentration

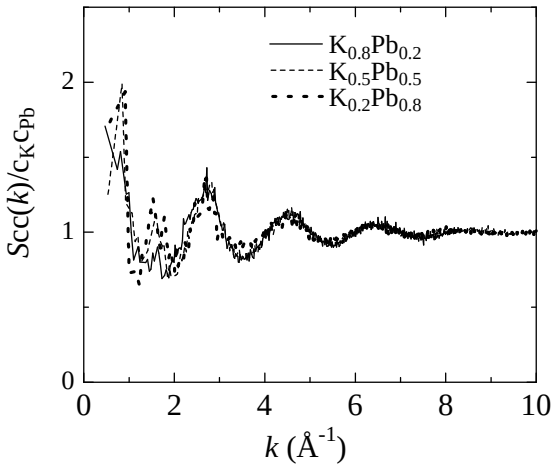

Figure 7. The concentration–concentration structure factors for the liquid $K_{0.8}Pb_{0.2}$ (solid curve), $K_{0.5}Pb_{0.5}$ (broken curve) and $K_{0.2}Pb_{0.8}$ (dotted curve) alloys.

fluctuation. According to Reijers *et al* [2], the combination of a prepeak and the tendency toward phase separation implies that there will be a K–Pb phase which is dominated by Pb clusters surrounded by K atoms as in the liquid $K_{0.5}Pb_{0.5}$ alloy, whereas the other phase consists mainly of K atoms. $S_{CC}(k)$ calculated by our simulation indicates an increase of the concentration fluctuation, though we cannot clearly confirm the tendency towards the phase separation as shown in figure 1. This is due to the limited size of the system used in our simulation.

3.2. Electronic properties

3.2.1. The electronic density of states. We calculate the total and partial densities of states (DOSs) by sampling ten k-points of the Brillouin zone and by averaging over some ionic configurations. The partial DOS of the ith species is calculated by projecting the wavefunctions on the spherical harmonics within a sphere of radius R_c centred at each atom of the ith species. R_c is 0.9 Å for K atoms and 0.8 Å for Pb atoms. The calculated total and partial DOSs are shown in figures 8 and 9. The origin of the energy is taken to be the Fermi level. The number of the electronic states obtained by integrating the total DOS increases with increasing number of Pb atoms, since a Pb atom has four valence electrons while a K atom has one valence electron.

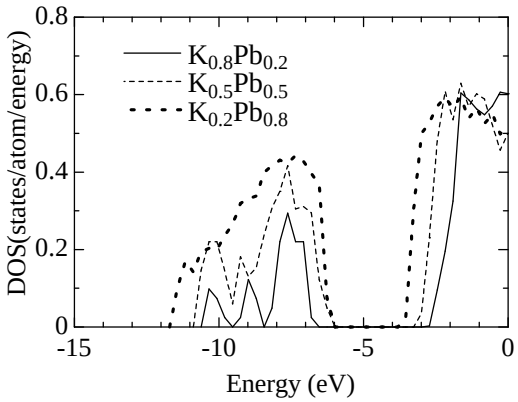

Figure 8. The total densities of states for the liquid $K_{0.8}Pb_{0.2}$ (solid curve), $K_{0.5}Pb_{0.5}$ (broken curve) and $K_{0.2}Pb_{0.8}$ (dotted curve) alloys.

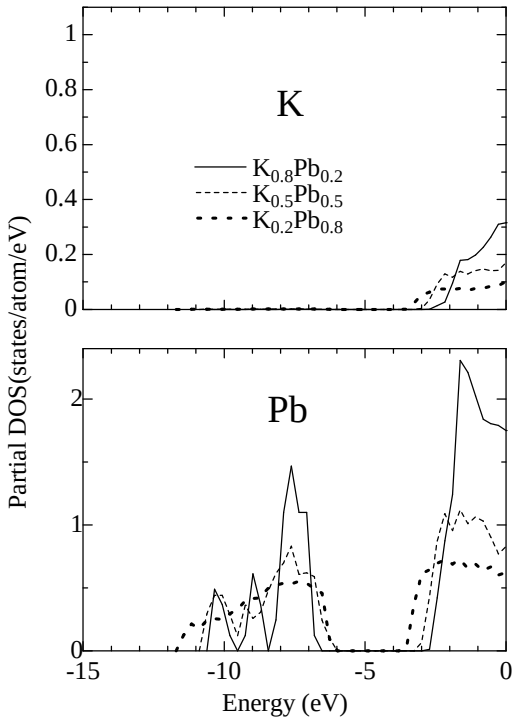

Figure 9. The partial densities of states for the liquid $K_{0.8}Pb_{0.2}$ (solid curves), $K_{0.5}Pb_{0.5}$ (broken curves) and $K_{0.2}Pb_{0.8}$ (dotted curves) alloys.

It is seen from the partial DOS for Pb that the band ranging from -12 eV to -6 eV, which arises from the Pb 6s states, becomes wider with increasing number of Pb atoms. This can be explained by associating it with the ionic structure as follows. For the K-rich alloy, the overlap of the wavefunction of the Pb 6s state is small for the ionic structure, which consists mainly of isolated Zintl ions and isolated Pb atoms. With increasing number of Pb atoms, the Zintl ions are connected with other Pb ions and the ionic structure of the Pb ions becomes denser, which leads to large degrees of overlap of Pb 6s wavefunctions and gives rise to the wider energy band.

It is seen from the partial DOS for K that the band consisting of K 4s states is similar to the nearly-free-electron (NFE) band for the liquid $K_{0.8}Pb_{0.2}$ alloy. With increasing Pb concentration, the band shifts to lower energy as a result of the hybridization of the Pb 6p states and the K 4s states, since the energy level of Pb 6p states is lower than that of the K 4s states.

3.2.2. The electrical conductivity. We show in figure 10 the electrical conductivities as functions of the frequency ($\sigma(\omega)$) calculated using the Kubo–Greenwood formula. The extrapolated values $\sigma(0)$ give the DC conductivities. In figure 11, the calculated resistivities ($=1/\sigma(0)$) are shown as a function of the composition. The observed composition dependence of the resistivity [4] shows a sharp maximum at $K_{0.5}Pb_{0.5}$, which is reproduced qualitatively, as is seen in figure 11. Drude-like behaviour is seen in the frequency dependence of the conductivity for the liquid $K_{0.8}Pb_{0.2}$ alloy, which is associated with the NFE-like structure of the K partial DOS of the liquid alloy.

The electronic properties are closely related to the ionic structures. For the liquid $K_{0.8}Pb_{0.2}$ alloy, isolated Zintl ions lead to a narrow Pb band, while the dominant K atoms have the NFE-like electronic structure near the Fermi level, which provides the main contribution

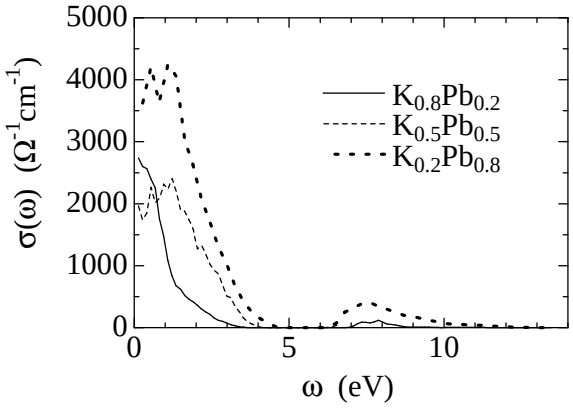

Figure 10. The electric conductivities as functions of ω for the liquid $K_{0.8}Pb_{0.2}$ (solid curve), $K_{0.5}Pb_{0.5}$ (broken curve) and $K_{0.2}Pb_{0.8}$ (dotted curve) alloys.

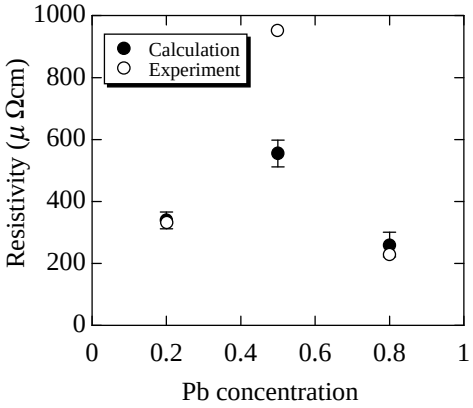

Figure 11. The electrical resistivities as a function of the composition.

to the conductivity. In the case of the liquid $K_{0.2}Pb_{0.8}$ alloy, on the other hand, the dense structure of the dominant Pb atoms forms a wide band, which is the main determinant of the conductivity. The liquid $K_{0.5}Pb_{0.5}$ alloy is a transitional case, where the tendency towards NFE-like character due to the K atoms is weak in comparison with that for the liquid $K_{0.8}Pb_{0.2}$ alloy, the concentration of the Pb ions is not so dense as is the case for the liquid $K_{0.2}Pb_{0.8}$ alloy and the randomness due to the mixing of the two components is the largest; as a result of these factors, the resistivity is the maximum for this alloy.

4. Summary

We have carried out *ab initio* molecular-dynamics simulations for the liquid K–Pb alloys to investigate the composition dependence of their ionic structure and electronic states, and obtained the following results:

(a) Tetrahedral Pb_4^{4-} clusters, which are the so-called 'Zintl ions' seen in the crystalline compound KPb, are seen clearly for the liquid K-rich alloy, while the Zintl ions are connected to each other and a complex structure is formed for the liquid equiatomic alloy.

(b) The observed structure factor characterized by the first sharp diffraction peak (FSDP) is reproduced and it is found that the FSDP originates from the intermediate-range ordering of the Zintl ions.

(c) The composition dependence of the resistivity is well reproduced by means of the Kubo–Greenwood formula and its characteristic features are understood on the basis of the calculated electronic states and the ionic structure obtained.

Acknowledgments

We are grateful to Professor M-L Saboungi for providing us with experimental data. We thank Mr Y Tsuchimoto for help in visualizing our data. This work was supported by Grant-in-Aids for Scientific Research (No 07236102, No 08304026 and No 10640370) from the Ministry of Education, Science, Sports and Culture, Japan. We thank the Computer Centre of the Institute for Molecular Science for allowing us to use the NEC SX-3/34R supercomputer. We also acknowledge the Centre for Promotion of Computational Science and Engineering (CCSE) of Japan Atomic Energy Research Institute (JAERI) for allowing us to use the NEC SX-4 and FUJITSU VPP300 supercomputers.

References

[1] Reijers H T J, Saboungi M-L, Price D-L, Richardson J W, Volin K J Jr and van der Lugt W 1989 *Phys. Rev.* B **40** 6018
[2] Reijers H T J, van der Lugt W, van Dijk C and Saboungi M-L 1989 *J. Phys.: Condens. Matter* **1** 5229
[3] Stolz M, Leichtweiss O, Winter R, Saboungi M-L, Fortner J and Howells W S 1994 *Europhys. Lett.* **27** 221
[4] Meijer J A, Vinke G J and van der Lugt W 1986 *J. Phys. F: Met. Phys.* **16** 845
[5] Geertsma W and van der Lugt W 1984 *J. Phys. F: Met. Phys.* **14** 1833
[6] de Wijs G A, Pastore G, Selloni A and van der Lugt W 1995 *J. Chem. Phys.* **103** 5031
[7] Senda Y, Shimojo F and Hoshino K 1999 *J. Phys.: Condens. Matter* **11** 2199
[8] de Wijs G A, Pastore G, Selloni A and van der Lugt W 1996 *J. Phys.: Condens. Matter* **8** 1879
[9] Holender J M and Gillan M J 1996 *Phys. Rev.* B **53** 4399
[10] Kirchhoff F, Holender J M and Gillan M J 1996 *Phys. Rev.* B **54** 190
[11] Seifert G, Kaschner R, Schöne M and Pastore G 1998 *J. Phys.: Condens. Matter* **10** 1175
[12] Seifert-Lorenz K and Hafner J 1999 *Phys. Rev.* B **59** 843
[13] Shimojo F, Hoshino K and Zempo Y 1999 *Phys. Rev.* B **59** 3514
[14] Senda Y, Shimojo F and Hoshino K 1998 *J. Phys. Soc. Japan* **67** 916
[15] Senda Y, Shimojo F and Hoshino K 1998 *J. Phys. Soc. Japan* **67** 2753
[16] Reijers H T A, van der Lugt W and Saboungi M-L 1990 *Phys. Rev.* B **42** 3395
[17] Alonso J A, Molina L M, López M J, Rubio A and Stott M J 1998 *Chem. Phys. Lett.* **289** 451
[18] Kresse G and Hafner J 1994 *Phys. Rev.* B **49** 14 251
[19] Shimojo F, Zempo Y, Hoshino K and Watabe M 1995 *Phys. Rev.* B **52** 9320
[20] Troullier N and Martins J L 1991 *Phys. Rev.* B **43** 1993
[21] Wood J H and Boring A M 1978 *Phys. Rev.* B **18** 2701
[22] Kleinman L and Bylander D M 1982 *Phys. Rev. Lett.* **48** 1425
[23] Ceperley D M and Alder B J 1980 *Phys. Rev. Lett.* **45** 566
[24] Perdew J P and Zunger A 1981 *Phys. Rev.* B **23** 5048
[25] Louie S G, Froyen S and Cohen M L 1982 *Phys. Rev.* B **26** 1738
[26] Nosé S 1984 *Mol. Phys.* **52** 255
[27] Hoover W G 1985 *Phys. Rev.* A **31** 1695